KIAS-P14051

Stop and Sbottom LSP with R-parity Violation

Eung Jin Chun,[1,*] Sunghoon Jung,[1,†] Hyun Min Lee,[2,‡] and Seong Chan Park[3,§]

[1]*Korea Institute for Advanced Study, Seoul 130-722, Korea*

[2]*Department of Physics, Chung-Ang University, Seoul 156-756, Korea*

[3]*Department of Physics, Sungkyunkwan University, Suwon 440-746, Korea*

Considering a third-generation squark as the lightest supersymmetric particle (LSP), we investigate R-parity violating collider signatures with bilinear LH or trilinear LQD operators that may contribute to observed neutrino masses and mixings. Reinterpreting the LHC $7+8$ TeV results of SUSY and leptoquark searches, we find that third-generation squark LSPs decaying to first- or second-generation leptons are generally excluded up to at least about 660 GeV at 95%C.L.. One notable feature of many models is that sbottoms can decay to top quarks and charged leptons that lead to a broader invariant mass spectrum and weaker collider constraints. More dedicated searches with b-taggings or top reconstructions are thus encouraged. Finally, we discuss that the recently observed excesses in the CMS leptoquark search can be accommodated by the decay of sbottom LSPs in the $\mathrm{LQD}_{113+131}$ model.

arXiv:1408.4508v2 [hep-ph] 2 Sep 2014

*Electronic address: ejchun@kias.re.kr

†Electronic address: nejsh21@gmail.com

‡Electronic address: hmlee@cau.ac.kr

§Electronic address: s.park@skku.edu

Contents

I. Introduction 2

II. Models with LH and LQD RPV 4
A. General Consideration 4
B. Benchmark Models 6

III. LHC Searches and Bounds 8

IV. The Observed Leptoquark Excess from Sbottom Decays 10
A. Sbottoms as Leptoquarks 11
B. Electroweak Precision Data and Stop Masses 12

V. Summary and Conclusion 14

A. Approximate Diagonalizations of RPV Masses 14

B. Bound Estimation 15

References 16

I. INTRODUCTION

Supersymmetry (SUSY) has been considered as a leading candidate for physics beyond the Standard Model because it provides a natural framework to stabilize the weak scale against huge quantum corrections. The CMS and ATLAS collaborations of the LHC experiment have been performing a broad range of searches for SUSY in various channels. After the LHC Run-1 with the $\sqrt{s} = 7, 8$ TeV collision energies, the first two generation squarks and gluinos are already excluded up to $1 \sim 2$ TeV and the third generation squarks up to $400 \sim 700$ GeV depending on various search channels with R-parity conservation (RPC) or violation (RPV) [1]. Among three generations of squarks, the third generation squarks are of particular interest, as they contribute significantly to the Higgs mass through loop corrections, and thus direct stop/sbottom searches at the LHC are motivated.

As is well-known, the Standard Model gauge invariance allows bilinear (LH) and trilinear (LLE, LQD) lepton-number (L) violating operators as well as trilinear (UDD) baryon-number (B) violating operators in the renormalizable superpotential:

$$W_{\rm RPV} = \epsilon_i \mu L H_u + \lambda_{ijk} L_i L_j E^c_k + \lambda'_{ijk} L_i Q_j D^c_k + \lambda''_{ijk} U^c_i D^c_j D^c_k \tag{1}$$

where μ denotes the supersymmetric mass parameter of the Higgs bilinear operator $H_u H_d$.

Simultaneous presence of λ' and λ'' makes proton unstable and thus has to be avoided. The proton stability may be ensured by imposing various discrete symmetries [2]. One of them is the standard R-parity forbidding all of the above operators.[1] Another popular options are to consider the B-parity and L-parity forbidding only B and L violating operators, respectively. The B-parity has an attractive feature that the allowed L violating operators could be the origin of tiny neutrino masses [3].

Motivated by these, we investigate signatures of stop/sbottom LSP directly decaying into a quark and a lepton through either the bilinear LH or trilinear LQD couplings which can contribute to the observed neutrino masses and mixing. One of the search channels for such RPV stop/sbottom is the conventional leptoquark search [4] which have been looked for at the HERA [5], and more recently at the LHC [6–9]. In this paper, we study various prompt multilepton and/or multijet signatures of the stop/sbottom LSP with the LH or LQD RPV to constrain the stop/sbottom mass combing all the relevant current LHC results not only from the leptoquark search but also from the RPC stop/sbottom as well as RPV multilepton searches. Our RPV models can have various types of couplings such as LH_i and $\mathrm{LQD}_{ij3,i3k}$, and the interpretation of data in terms of these variant models can be different. The L violating RPV signatures of stop have been studied earlier in Refs. [10], and more recently in Ref. [11]. Leptoquark signatures of stop/sbottom LSP have also been explored recently in Ref. [12] in the context of a bilinear spontaneous RPV model.

The CMS has also reported excesses in the leptoquark mass range of $600 - 700$ GeV in both $eejj$ and $e\nu jj$ channels with 2.4σ and 2.6σ, respectively [7]. These excesses are characterized by jets from non-b quarks. On the other hand, no similar excess is observed in $\mu\mu(\nu)jj$ and $\tau\tau(\nu)jj$ channels. It is attempting to see if such observed signatures are understood by any of RPV stop/sbottom LSP decay processes. Interestingly, these excesses can be accommodated in the sbottom LSP scenario with appropriate LQD operators. This may have some implication on the other stop/sbottom masses from the electroweak precision data (EWPD). One can find other attempts to explain the excess in Refs. [13].

This paper is organized as follows. We start by deriving the stop/sbottom RPV vertices arising from the LH and LQD couplings and reviewing their implication to the neutrino mass matrix, and then we set up benchmark models specified by various LH and LQD couplings in Sec. II. Various LHC 7+8 TeV results are reinterpreted to constrain these benchmark models in Sec. III. Several qualitatively different models are considered and dedicated searches are proposed. The comparison with RPC model constraints is another useful result of this paper. Sec. IV addresses the issue of accommodating the recently observed mild excesses

[1] Note that the dimension-5 B and L violating operator $LQQQ$, which is R-parity even, is assumed to be highly suppressed in addition.

in the CMS leptoquark searches in our context, and its possible implication to EWPD constraints. Finally we conclude in Sec. V.

II. MODELS WITH LH AND LQD RPV

A. General Consideration

As mentioned, we consider the LH and LQD operators relevant for the stop and sbottom LSP decays:

$$W_{\rm RPV} = \epsilon_i \mu L_i H_u + \lambda'_{ijk} L_i Q_j D^c_k \,. \tag{2}$$

LH: Let us first derive the stop and sbottom couplings arising from the bilinear LH RPV. For this, we need to include also soft SUSY breaking bilinear terms,

$$V_{\rm soft,LH} \;=\; B_i L_i H_u \;+\; m^2_{L_i H_d} L_i H^\dagger_d \;+\; h.c., \tag{3}$$

which generate the vacuum expectation value (vev) of a sneutrino field $\tilde{\nu}_i$ parameterized as $\langle\tilde{\nu}_i\rangle \equiv a_i \langle H_d\rangle$ with $a_i = (B_i t_\beta + m^2_{L_i H_d})/m^2_{\tilde{\nu}_i}$. Here t_β is the ratio between two Higgs vevs: $t_\beta = \langle H^0_u\rangle/\langle H^0_d\rangle$ The bilinear couplings ϵ_i and a_i induce mixing masses between neutrinos (charged leptons) and neutralinos (charginos) and thereby non-vanishing neutrino masses as well as effective RPV couplings of the stop and sbottom LSP of our interest. To see this, it is convenient to diagonalize away first these mixing masses as discussed in Ref. [14]. The relevant approximate diagonalizations valid in the limit of $\epsilon_i, a_i \ll 1$ are collected in Appendix A. After these diagonalizations, we get the following RPV vertices of stops:

$$-\mathcal{L} \;=\; \tilde{t}_L \bar{t} \left(\kappa^t_{L\nu_i} P_L + \kappa^t_{R\nu_i} P_R\right) \nu_i + \tilde{t}_R \bar{t} \left(\rho^t_{L\nu_i} P_L + \rho^t_{R\nu_i} P_R\right) \nu_i + h.c. \tag{4}$$

$$+\; \tilde{t}_L \bar{b} \left(\kappa^t_{Le_i} P_L + \kappa^t_{Re_i} P_R\right) e_i + \tilde{t}_R \bar{b} \left(\rho^t_{Le_i} P_L + \rho^t_{Re_i} P_R\right) e_i + h.c., \tag{5}$$

where

$$\kappa^t_{L\nu_i} = y_t c^N_4 \xi_i c_\beta \,, \qquad \kappa^t_{R\nu_i} = (\frac{\sqrt{2}}{6} g' c^N_1 + \frac{1}{\sqrt{2}} g c^N_2) \xi_i c_\beta, \tag{6}$$

$$\rho^t_{L\nu_i} = \frac{2\sqrt{2}}{3} g' c^N_1 \xi_i c_\beta \,, \qquad \rho^t_{R\nu_i} = y_t c^N_4 \xi_i c_\beta, \tag{7}$$

$$\kappa^t_{Le_i} = -y_b c^L_2 \xi_i c_\beta + y_b \epsilon_i \,, \quad \kappa^t_{Re_i} = g \frac{m^e_i}{F_C} c^R_1 \xi_i c_\beta, \tag{8}$$

$$\rho^t_{Le_i} = 0 \,, \qquad \rho^t_{Re_i} = -y_t \frac{m^e_i}{F_C} c^R_2 \xi_i c_\beta. \tag{9}$$

Similarly, the sbottom RPV vertices are given by

$$
\begin{aligned}
-\mathcal{L} &= \tilde{b}_L \bar{b} \left(\kappa^b_{L\nu_i} P_L + \kappa^b_{R\nu_i} P_R\right) \nu_i + \tilde{b}_R \bar{b} \left(\rho^b_{L\nu_i} P_L + \rho^b_{R\nu_i} P_R\right) \nu_i + h.c. && (10)\\
&+ \tilde{b}_L \bar{t} \left(\kappa^b_{Le_i} P_L + \kappa^b_{Re_i} P_R\right) e_i + \tilde{b}_R \bar{t} \left(\rho^b_{Le_i} P_L + \rho^b_{Re_i} P_R\right) e_i + h.c., && (11)\\
\text{where} \quad & \kappa^b_{L\nu_i} = y_b c_3^N \xi_i c_\beta - y_b \epsilon_i \,, \quad \kappa^b_{R\nu_i} = (\frac{\sqrt{2}}{6} g' c_1^N - \frac{1}{\sqrt{2}} g c_2^N) \xi_i c_\beta, && (12)\\
& \rho^b_{L\nu_i} = -\frac{\sqrt{2}}{3} g' c_1^N \xi_i c_\beta \,, \qquad \rho^b_{R\nu_i} = y_b c_3^N \xi_i c_\beta - y_b \epsilon_i, && (13)\\
& \kappa^b_{Le_i} = -y_t \frac{m^e_i}{F_C} c_2^R \xi_i c_\beta \,, \qquad \kappa^b_{Re_i} = g \frac{m^e_i}{F_C} c_1^R \xi_i c_\beta, && (14)\\
& \rho^b_{Le_i} = 0 \,, \qquad \rho^b_{Re_i} = -y_b c_2^L \xi_i c_\beta + y_b \epsilon_i. && (15)
\end{aligned}
$$

LQD: It is straightforward to get the stop and sbottom RPV vertices coming from the trilinear RPV couplings, λ'_{ijk} with j or $k = 3$:

$$
\begin{aligned}
-\mathcal{L} &= \lambda'_{i33} \left(\tilde{b}_L \bar{b} P_L \nu_i + \tilde{b}_R \bar{b} P_R \nu_i - \tilde{t}_L \bar{b} P_L e_i - \tilde{b}_R \bar{t} P_R e_i\right) + h.c. && (16)\\
&+ \lambda'_{ij3} \left(\tilde{b}_R \bar{d}_j P_R \nu_i - \tilde{b}_R \bar{u}_j P_R e_i\right) + h.c. && (17)\\
&+ \lambda'_{i3k} \left(\tilde{b}_L \bar{d}_k P_L \nu_i - \tilde{t}_L \bar{d}_k P_L e_i\right) + h.c.. && (18)
\end{aligned}
$$

When the LH and LQD PRV are allowed, their couplings can contribute to generate neutrino mass matrix components respectively at tree and one-loop (see Fig. 1) as follows:

$$
\begin{aligned}
m^{\text{tree}}_{\nu,ij} &= \frac{M_Z^2}{F_N} \xi_i \xi_j c_\beta^2 \,, && (19)\\
m^{\text{loop}}_{\nu,ij} &= \sum_{k=1}^{3} \frac{3}{16\pi^2} (\lambda'_{ik3} \lambda'_{j3k} + \lambda'_{i3k} \lambda'_{jk3}) \frac{m_{d_k} m_b X_b}{m^2_{\tilde{b}_2} - m^2_{\tilde{b}_1}} \ln \frac{m^2_{\tilde{b}_2}}{m^2_{\tilde{b}_1}}, && (20)
\end{aligned}
$$

where $m_b X_b$ is the sbottom mixing mass-squared and only sbottom contributions are included assuming $m_{\tilde{b}} \ll m_{\tilde{d}_k}$ for $k = 1, 2$. A complete 1-loop calculation can be found in Refs. [14, 15]. In the case of the neutralino LSP, the RPV signatures correlated with the neutrino mixing angles have been extensively studied [16–18] as well as in the split SUSY [19]. Similar studies are worthwhile in the case of the stop/sbottom LSP as well. We leave this issue as a future work.

From the expressions in Eqs. (19, 20), the LH and LQD couplings are constrained by the measured values of tiny neutrino masses. As a rough estimate, the following bilinear and trilinear couplings are required to generate the neutrino mass components of $m_{\nu,ii} = 0.01$

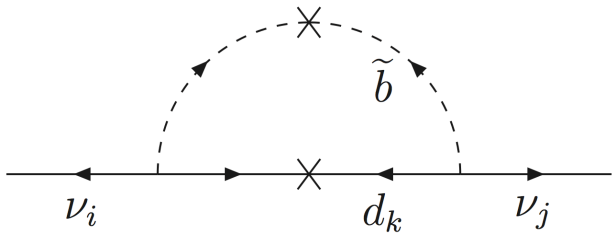

FIG. 1: Feynman diagrams responsible for neutrino mass generation, $m_{\nu,ij}$, through light sbottoms and LQD couplings $\lambda'_{ik3}\lambda'_{j3k}$.

eV:

$$|\xi_i c_\beta| \approx 10^{-6}\,, \tag{21}$$

$$|\lambda'_{ik3}\lambda'_{i3k}|^{1/2} \approx 3.4\times 10^{-3}\sqrt{\frac{m_d}{m_{d_k}}}, \tag{22}$$

taking $F_N = X_b = \sqrt{(m^2_{\tilde{b}_2} - m^2_{\tilde{b}_1})/\ln(m^2_{\tilde{b}_2}/m^2_{\tilde{b}_1})} = 1$ TeV. These coupling sizes are small enough that they do not affect production rates and do not make resonances broader than experimental resolutions so that collider physics is mostly independent on them. Nevertheless, they are large enough to allow prompt decays of squark LSPs.

B. Benchmark Models

We now introduce three benchmark models. Sbottom and stop LSPs decay to either first- or second-generation leptons. Model names imply the involved RPV interactions and subscripts imply lepton and/or quark generations.

In the presence of the mixing between left-handed and right-handed stops/sbottoms, we can write the stop/sbottom mass eigenstates, $\tilde{q}_1$ and $\tilde{q}_2$ with $q = t, b$:

$$\tilde{q}_L \;=\; \cos\theta_{\tilde{q}}\,\tilde{q}_1 - \sin\theta_{\tilde{q}}\,\tilde{q}_2, \tag{23}$$

$$\tilde{q}_R \;=\; \sin\theta_{\tilde{q}}\,\tilde{q}_1 + \cos\theta_{\tilde{q}}\,\tilde{q}_2, \tag{24}$$

where $\theta_{\tilde{q}}$ is the squark mixing angle. We are interested in the RPV vertices of the lightest stop ($\tilde{t}_1$) or sbottom ($\tilde{b}_1$).

$\underline{\text{LH}_i}$: Stop and sbottom decay modes are $\tilde{b}_1 \to e_i t, \nu_i b$ and $\tilde{t}_1 \to e_i b, \nu_i t$, and the branching

fraction for the charged lepton modes are given by (ignoring top and bottom masses)

$$\beta_{\tilde{b}} \equiv \mathrm{BR}(\widetilde{b}_1 \to e_i t) \approx \frac{\sin^2\theta_{\tilde{b}}|\rho^b_{Re_i}|^2}{|\kappa^b_{L\nu_i}|^2 + \cos^2\theta_{\tilde{b}}|\kappa^b_{R\nu_i}|^2 + \sin^2\theta_{\tilde{b}}|\rho^b_{L\nu_i}|^2 + \sin^2\theta_{\tilde{b}}|\rho^b_{Re_i}|^2}, \quad (25)$$

$$\beta_{\tilde{t}} \equiv \mathrm{BR}(\widetilde{t}_1 \to e_i b) \approx \frac{\cos^2\theta_{\tilde{t}}|\kappa^t_{Le_i}|^2}{|\kappa^t_{L\nu_i}|^2 + \cos^2\theta_{\tilde{t}}|\kappa^t_{R\nu_i}|^2 + \sin^2\theta_{\tilde{t}}|\rho^t_{L\nu_i}|^2 + \cos^2\theta_{\tilde{t}}|\kappa^t_{Le_i}|^2}, \quad (26)$$

where we neglect the terms suppressed by m^e_i/F_C. As the stop or the sbottom is the LSP, it is expected to have $M_Z \ll \mu$ and thus $|c^N_{3,4}, c^{L,R}_2| \ll |c^N_{1,2}, c^{L,R}_1|$, which leads to

$$\beta_{\tilde{b}} \approx \frac{\sin^2\theta_{\tilde{b}}|y_b\epsilon_i|^2}{\left[\cos^2\theta_{\tilde{b}}|\frac{\sqrt{2}}{6}g'c^N_1 - \frac{1}{\sqrt{2}}gc^N_2|^2 + \sin^2\theta_{\tilde{b}}|\frac{\sqrt{2}}{3}g'c^N_1|^2\right]|\xi_i c_\beta|^2 + (1+\sin^2\theta_{\tilde{b}})|y_b\epsilon_i|^2}, \quad (27)$$

$$\beta_{\tilde{t}} \approx \frac{\cos^2\theta_{\tilde{t}}|y_b\epsilon_i|^2}{\left[\cos^2\theta_{\tilde{t}}|\frac{\sqrt{2}}{6}g'c^N_1 + \frac{1}{\sqrt{2}}gc^N_2|^2 + \sin^2\theta_{\tilde{t}}|\frac{2\sqrt{2}}{3}g'c^N_1|^2\right]|\xi_i c_\beta|^2 + \cos^2\theta_{\tilde{t}}|y_b\epsilon_i|^2}. \quad (28)$$

Note that the LH model becomes effectively equivalent to the LQD_{i33} model with $\lambda'_{i33} \equiv \epsilon_i y_b$ (see below) in the limit of vanishing ξ_i.

$\underline{\mathrm{LQD}_{i33}}$: Only $\lambda'_{i33} \neq 0$ is assumed to allow the decay modes $\tilde{b}_1 \to e_i t, \nu_i b$ or $\tilde{t}_1 \to e_i b$. Thus, the sbottom and stop decay branching ratios for the charged lepton modes are

$$\beta_{\tilde{b}} \equiv \mathrm{BR}(\widetilde{b}_1 \to e_i t) = \frac{\sin^2\theta_{\tilde{b}}}{1+\sin^2\theta_{\tilde{b}}}, \quad (29)$$

$$\beta_{\tilde{t}} \equiv \mathrm{BR}(\widetilde{t}_1 \to e_i b) = 1\,. \quad (30)$$

$\underline{\mathrm{LQD}_{ij3+i3j}}$: Only $\lambda'_{ij3,\,i3j} \neq 0$ is assumed to allow $\tilde{b}_1 \to e_i u_j, \nu_i d_j$ or $\tilde{t}_1 \to e_i d_j$. The sbottom and stop branching ratios for the charged lepton modes are

$$\beta_{\tilde{b}} \equiv \mathrm{BR}(\widetilde{b}_1 \to e_i u_j) = \frac{\sin^2\theta_{\tilde{b}}|\lambda'_{ij3}|^2}{\cos^2\theta_{\tilde{b}}|\lambda'_{i3j}|^2 + 2\sin^2\theta_{\tilde{b}}|\lambda'_{ij3}|^2}, \quad (31)$$

$$\beta_{\tilde{t}} \equiv \mathrm{BR}(\widetilde{t}_1 \to e_i d_j) = 1\,. \quad (32)$$

The first two models, LH_i and LQD_{i33}, involve heavy quarks (tops and bottoms) in the final states while only light quarks are produced in the $\mathrm{LQD}_{ij3+i3j}$ model.

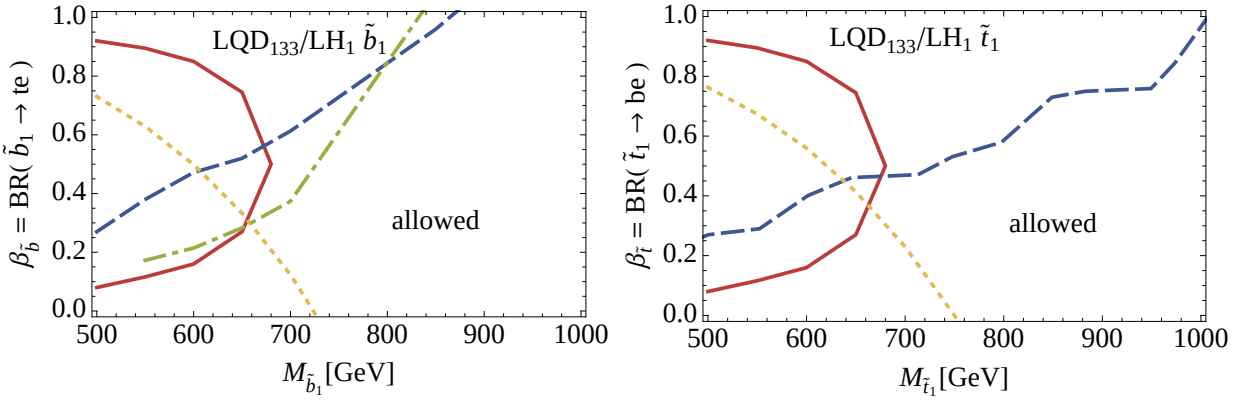

FIG. 2: 95%C.L. Exclusion plots for the sbottom LSP (**left**) and the stop LSP (**right**) from CMS leptoquark searches in $eejj$ (blue-dashed) and $e\nu jj$ (red-solid) channels. Also shown are CMS RPC sbottom and stop searches (yellow-dotted) in $b\bar{b}$+MET and $t\bar{t}$+MET channels. For sbottoms, CMS multilepton ($\geq 3\ell$) RPV search constrains additionally (green-dot-dashed). The region left to each line is excluded. The bounds are equally applicable to LH_1 and LQD_{133} models.

III. LHC SEARCHES AND BOUNDS

Let us first consider how the sbottom LSP can be constrained at the LHC. Sbottom pair productions in the LH_1 and LQD_{133} models, leave the final states:

$$\widetilde{b}_1\widetilde{b}_1^* \to bb\nu\nu,\ tbe\nu,\ ttee. \tag{33}$$

The $bb\nu\nu$ is constrained by RPC sbottom searches through $\widetilde{b}_1 \to b\chi_1^0$ with the massless LSP, hence $b\bar{b}$+missing transverse energy(MET). The existing strongest bound on the sbottom mass is 725GeV from CMS 19.4/fb [20]. The $tbe\nu$ can be constrained from the $e\nu jj$ searches of first-generation leptoquarks [7] – the CMS analysis uses two hardest jets of any flavor. Note that the sbottom and the leptoquark have the same quantum numbers as color triplet, and their production rates are almost identical, as dictated by QCD interactions. So it is appropriate to use this result to extract bounds on sbottoms. The $ttee$ can be constrained from the $eejj$ searches of leptoquarks and additionally from multi-lepton($\geq 3\ell$) RPV LLE searches [21]. We comment on other searches in Appendix B.

We recast these search results to exclusion bounds on the sbottom in the left panel of Fig. 2 – we refer to Appendix B for how we obtain these bounds. The same bounds apply to both LQD_{133} and LH_1 as they predict the same final states. Large $\beta_{\tilde{b}}$ is constrained from the $eejj$ and the multi-lepton RPV searches whereas small $\beta_{\tilde{b}}$ is constrained from the RPC sbottom search. In general, sbottoms lighter than about 660 GeV is excluded by at least one of those searches.

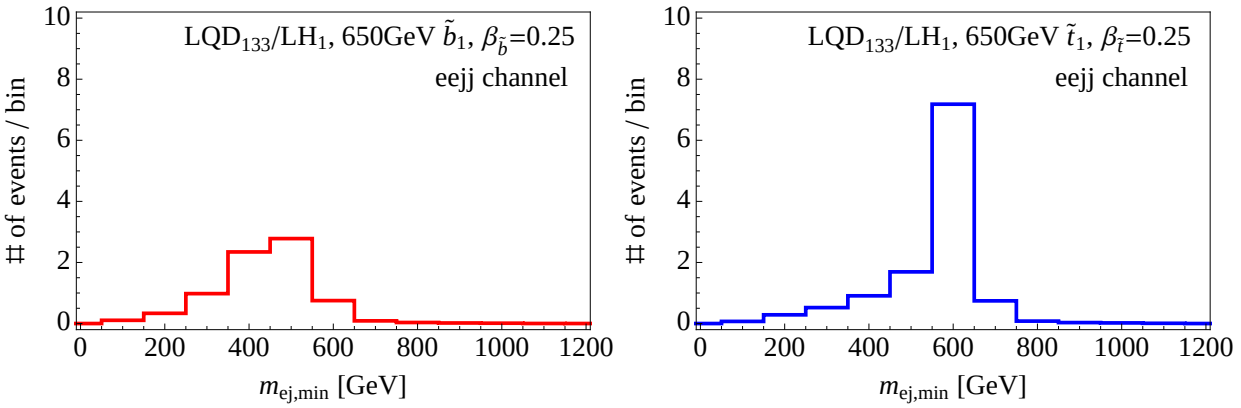

FIG. 3: Invariant mass, $m_{ej,\min}$, from 650GeV sbottom(**left**) or stop(**right**) pairs decaying to $eejj$ channel via LH_1 or LQD_{133} RPV couplings. CMS leptoquark search cuts are applied except for the cut on the invariant mass. 19.6/fb is assumed. $\beta = 0.25$ is chosen for illustration.

We now turn to the stop LSP. Stop pairs in the LH_1 and LQD_{133} models decay as

$$\widetilde{t}_1\widetilde{t}_1^* \to tt\nu\nu,\ tbe\nu,\ bbee, \tag{34}$$

where the first two modes are not allowed in the LQD_{133} model. The $tt\nu\nu$ channel is constrained by RPC stop searches through $\widetilde{t}_1 \to t\chi_1^0$ with the massless LSP. The existing strongest bound is 750 GeV from CMS 19.5/fb [22]. The remaining decay modes, $tbe\nu$ and $bbee$, can be constrained from the $e\nu jj$ and $eejj$ searches of first-generation leptoquarks [7]. Note that the stop also has the same quantum numbers as leptoquarks. Unlike sbottoms, stop pairs do not lead to final states with more than 3 leptons. Recasting these search results to exclusion bounds on the stop, we obtain the right panel of Fig. 2. Similarly to the sbottom case, stops lighter than about 660 GeV is excluded.

There is one notable difference between the sbottom LSP and the stop LSP. Sbottom pairs decay to $ttee$ while stop pairs decay to $bbee$. Tops produce more jets, and each jet becomes softer as decay products share the energy-momentum of sbottoms. Thus the acceptance under leptoquark search cuts gets lower. The $eejj$ exclusion bound (blue-dashed) on sbottoms (the left panel of Fig. 2) is indeed weaker than that on stops (the right panel of Fig. 2). Likewise, the $e\nu jj$ bound (red solid) in Fig. 2 is also weaker than the official $e\nu jj$ bound on the leptoquark model in Ref. [7].

Most notably, the invariant mass of the ej pair, $m_{ej,\min}$, does not reconstruct the sbottom mass. In Fig. 3, we contrast the invariant mass spectrum for the sbottom LSP and the stop LSP. We choose the presumably correct ej pair according to the CMS leptoquark analysis; the pair giving smaller invariant mass difference is selected. The m_{ej} from sbottoms have a broader spectrum and the peak formed at a lower mass because not all top decay products

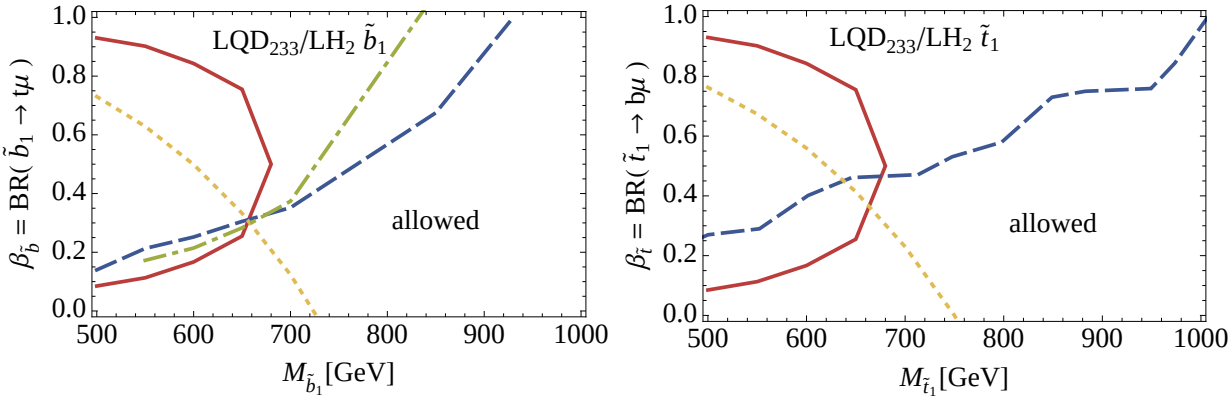

FIG. 4: Same as in Fig. 2 but the μ channel results of CMS leptoquark searches [8] are used for the red-solid and blue-dashed lines, which constrain the models LH_2 and LQD_{233} models.

are included. It will be useful to measure this characteristic difference in the future searches.

Therefore, potentially significant improvements in the third-generation squark LSP searches can be achieved with b-taggings and/or top reconstructions. With 20/fb of data, 8.1fb $\times$ 20/fb $\simeq$ 160 pairs of 700 GeV sbottoms are produced, and much better bounds are beginning to be statistically limited. In any case, 160 is still a reasonably large number, and more dedicated searches implementing b-tagging and/or top reconstruction are certainly worthwhile.

We can repeat the same analysis in the LH_2 and LQD_{233} models allowing sbottom and stop LSP decays to μ, and apply the CMS second-generation leptoquark searches [8]. The resulting bounds are shown in Fig. 4. Compared to the $eejj$ search, the $\mu\mu jj$ search is somewhat more stringent partly because μ is more accurately measured and cleaner – compare blue-dashed lines in the left panels of Fig. 2 and Fig. 4. On the other hand, $\mu\nu jj$ results are similar to $e\nu jj$ results (red-solid lines). To summarize, again, third-generation squark LSPs lighter than about 660 GeV are generally excluded.

Finally, the $LQD_{ij3+i3j}$ models with $i, j = 1, 2$ are equivalent to the leptoquark models and the current search results can be directly applied to constrain the sbottom/stop LSP mass.

IV. THE OBSERVED LEPTOQUARK EXCESS FROM SBOTTOM DECAYS

The CMS leptoquark analysis has recently reported excesses in 650GeV leptoquark searches in both $eejj$ and $e\nu jj$ channels [7]. The excesses are claimed to be 2.4 and 2.6σ significant, respectively. The excesses disappear when a b-jet is required, and no similar excess is observed in searches with μ [8] and τ [9]. In this section, we discuss how our third

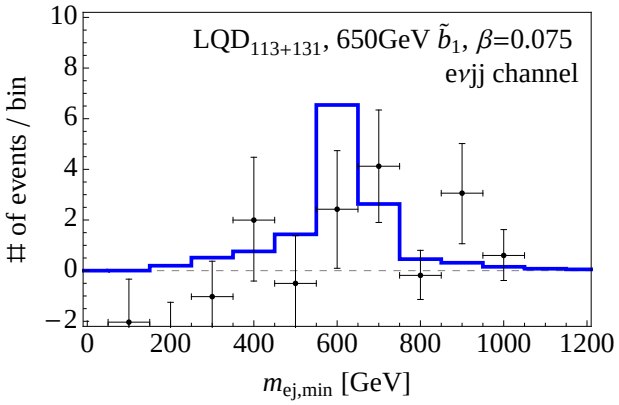

FIG. 5: The invariant mass, $m_{ej,\min}$, from 650GeV sbottom pairs decaying to the $e\nu jj$ channel via $\mathrm{LQD}_{113+131}$ RPV couplings. CMS leptoquark search cuts are applied except for the cut on the invariant mass. 19.6/fb is assumed. A small $\beta = 0.075$ giving a good fit to data is chosen. The data with SM predictions subtracted are taken from CMS results in Ref. [7].

model, $\mathrm{LQD}_{113+131}$, can fit the excesses.

A. Sbottoms as Leptoquarks

Sbottom pairs in the $\mathrm{LQD}_{113+131}$ model decay as

$$\widetilde{b}_1 \widetilde{b}_1^* \to dd\nu\nu,\ due\nu,\ uuee, \tag{35}$$

with BR$=(1-\beta)^2$, $2\beta(1-\beta)$ and β^2, respectively. This model is identical to the first-generation leptoquark model considered in the CMS analysis except that β is given differently by Eq. (31) in our model. The best fit is allegedly reported to be with 650 GeV and $\beta = 0.075$. Our model can accommodate this by the decay of sbottom LSPs. By simply assuming $\lambda'_{113} = \lambda'_{131}$ as an example, we can extract more specific information on the underlying parameters. Then, $\beta = \sin^2\theta_{\tilde{b}}/(1+\sin^2\theta_{\tilde{b}}) \leq 0.5$ is now bounded from above. The best-fit value, $\beta = 0.075$, requires $\sin^2\theta_{\tilde{b}} = 0.081$, meaning that the sbottom LSP is mostly left-handed. The constraint from electroweak precision test is briefly discussed in the next subsection.

The $m_{ej,\min}$ invariant mass spectrum is also scrutinized in the CMS analysis. So far, no sharp peak is observed unlike the expectation from leptoquark decays. As compared to our previous two models, the $\mathrm{LQD}_{113+131}$ does not involve top quarks and would also predict the same sharp peak in the invariant mass as leptoquark model does. See Fig. 5 for the comparison of the model prediction and data – no clear resonance-like structure is seen in data, but the model prediction is not significantly different from data yet.

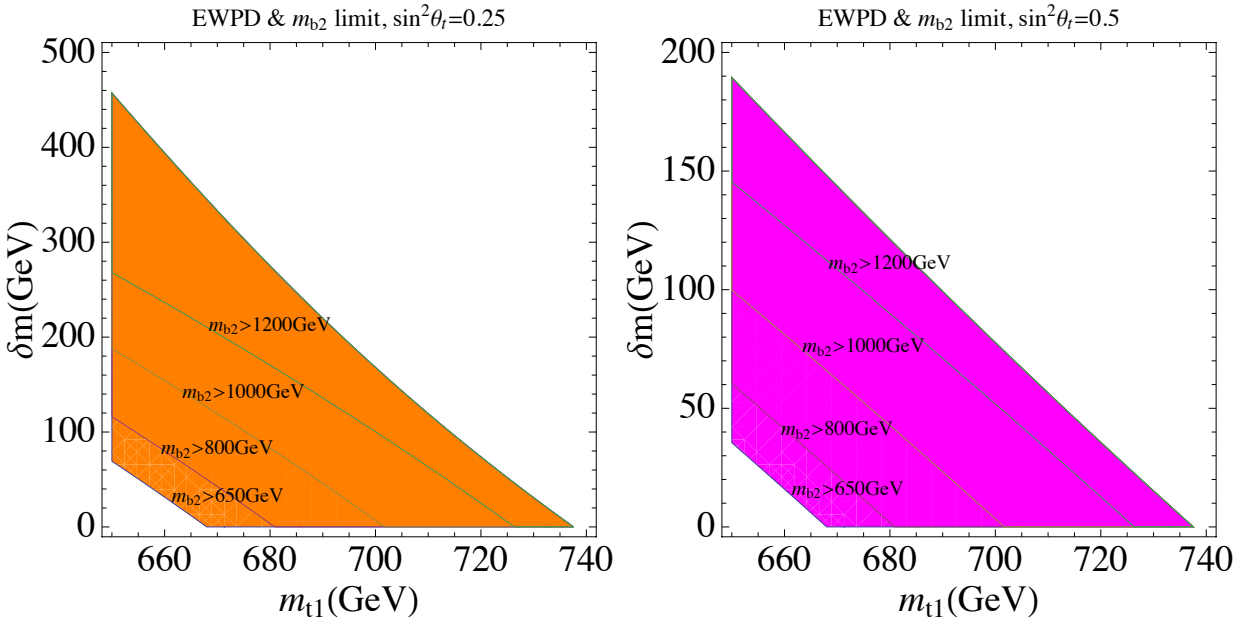

FIG. 6: The EWPD constraints on stop and heavy sbottom masses for the best-fit parameters, with 650 GeV sbottom LSP and $\sin^2\theta_{\tilde{b}} = 0.081$. Here, $\delta m \equiv m_{\tilde{t}_2} - m_{\tilde{t}_1}$ is the stop mass splitting. Lighter stop mass is bounded by EWPD and the stop mass splitting scales up as the bound on the heavier sbottom mass increases. In both figures, $\tan\beta = 10$ is chosen.

Our interpretation of the sbottom LSP in the $\text{LQD}_{113+131}$ model as a leptoquark of 650 GeV responsible for the mild CMS excesses requires the corresponding couplings, λ'_{113} and λ'_{131}, to dominate over other sbottom LSP RPV couplings if any. As discussed in Eq. (21,22), these couplings can take the values of $\lambda'_{113} \sim \lambda'_{131} \sim 10^{-3}$ to produce (mainly) the (11) component of the observed neutrino mass matrix. Then, the other components can come from smaller bilinear RPV couplings $\xi_i c_\beta \sim 10^{-6}$ and/or trilinear couplings, e.g., $\lambda'_{i33} \sim 10^{-4}$ to produce $m^{\text{tree}}_{\nu,ij} \propto \xi_i \xi_j c^2_\beta$ and/or $m^{\text{loop}}_{\nu,ij} \propto \lambda'_{i33}\lambda'_{j33}$. In this scenario, the sbottom LSP can have additional but suppressed decay modes in the μ and τ channels which may provide a test of the model. Of course, the neutrino mass components can come mainly from the LLE couplings, e.g., $m^{\text{loop}}_{\nu,ij} \propto \lambda_{i33}\lambda_{j33}$, which has no impact on the sbottom LSP phenomenology.

B. Electroweak Precision Data and Stop Masses

The mostly left-handed sbottom solution obtained in the previous subsection may imply that other stops (and/or sbottoms) are also light; otherwise, the model is inconsistent with the electroweak precision data(EWPD). The possible other light particles can provide additional collider constraints on the model. Indeed, it has been shown that the EWPD can give important constraints on the stop masses and mixing angles in combination with the RPC searches of sbottoms [23].

The deviation from the custodial symmetry in the SM is bounded to [24]

$$\begin{aligned}(\Delta\rho_0)^{\pm} &= (\rho_0)_{m_h=125\,\mathrm{GeV}} - 1 \\ &= (4.2 \pm 2.7) \times 10^{-4}.\end{aligned} \tag{36}$$

The sbottom and stop contribution to the ρ parameter [25] is

$$\begin{aligned}\Delta\rho_0^{SUSY} = \frac{3G_\mu}{8\sqrt{2}\pi^2}\Big[&- \sin^2\theta_{\tilde{t}}\cos^2\theta_{\tilde{t}}F_0(m^2_{\tilde{t}_1}, m^2_{\tilde{t}_2}) - \sin^2\theta_{\tilde{b}}\cos^2\theta_{\tilde{b}}F_0(m^2_{\tilde{b}_1}, m^2_{\tilde{b}_2}) \\ &+ \cos^2\theta_{\tilde{t}}\cos^2\theta_{\tilde{b}}F_0(m^2_{\tilde{t}_1}, m^2_{\tilde{b}_1}) + \cos^2\theta_{\tilde{t}}\sin^2\theta_{\tilde{b}}F_0(m^2_{\tilde{t}_1}, m^2_{\tilde{b}_2}) \\ &+ \sin^2\theta_{\tilde{t}}\cos^2\theta_{\tilde{b}}F_0(m^2_{\tilde{t}_2}, m^2_{\tilde{b}_1}) + \sin^2\theta_{\tilde{t}}\sin^2\theta_{\tilde{b}}F_0(m^2_{\tilde{t}_2}, m^2_{\tilde{b}_2})\Big],\end{aligned} \tag{37}$$

where F_0 is defined by

$$F_0[x,y] = x + y - \frac{2xy}{x-y}\log\frac{x}{y}. \tag{38}$$

From the mass terms for stops and sbottoms, we can infer the following relation between physical squark masses and mixing angles,

$$\sin^2\theta_{\tilde{b}}\, m^2_{\tilde{b}_2} + \cos^2\theta_{\tilde{b}}\, m^2_{\tilde{b}_1} = \cos^2\theta_{\tilde{t}}\, m^2_{\tilde{t}_1} + \sin^2\theta_{\tilde{t}}\, m^2_{\tilde{t}_2} - m_t^2 - m_W^2\cos(2\beta) + m_b^2. \tag{39}$$

In Fig. 6, we show bounds on the masses of other sbottoms and stops by assuming the best-fit parameters, $m_{\tilde{b}_1} = 650$ GeV and $\sin^2\theta_{\tilde{b}} = 0.081$, chosen in the previous subsection. Although the EWPD bound depends on various other parameters including stop mixing angle, the lighter stop mass is bounded up to about 740 GeV and the stop mass splitting is bounded up to about 190 GeV for a maximal stop mixing. In particular, when the collider limit on the heavier sbottom mass increases, the lighter stop mass and the stop mass splitting tend to get larger so the allowed parameter space in the stop sector is reduced.

The 125 GeV Higgs mass would require stop masses of $500 - 800$ GeV for a maximal stop mixing or stop masses above 3 TeV for a zero stop mixing [26]. Thus, in the case of a small stop mixing, the Higgs mass condition would be incompatible with EWPD. On the other hand, for a maximal stop mixing, the stop masses required for the Higgs mass can constrain the parameter space further. When there is a new dynamics for enhancing the Higgs mass such as a singlet chiral superfield, we may take the EWPD in combination with sbottom mass limit to be a robust bound on stop masses.

V. SUMMARY AND CONCLUSION

Through LH and LQD RPV couplings, the third-generation squark LSP can decay to leptons and jets. Jet+MET final states are constrained by conventional RPC SUSY searches, and multilepton(+jets)+MET final states are constrained from leptoquark searches as well as multilepton RPV searches. We found that the sbottom and the stop LSP decaying to e or μ are similarly well constrained up to about $0.66 \sim 1$ TeV depending on leptonic branching fractions. When the sbottom decays to a top quark and an electron as in the LH_i and LQD_{i33} models, the bounds are slightly weaker as each top decay product is softer and not all is used in the analyses. The resulting characteristically different m_{ej} invariant mass spectra can distinguish the models. More dedicated search for this case can be pursued by implementing b-taggings and/or top reconstructions. The bounds on μ final states are somewhat stronger than those on e final states so that a wider region of parameter space above 660 GeV is excluded for the LH_2 and LQD_{233} models. Lastly, we proposed the $\mathrm{LQD}_{113+131}$ model with sbottom LSPs as a good fit to the recently observed mild leptoquark excesses and discussed its possible implications on the masses of other stops and sbottoms in view of the EWPD and the 125 GeV Higgs mass.

Acknowledgement. We thank Suyong Choi for helpful comments. E.J.C is supported by the NRF grant funded by the Korea government (MSIP) (No. 2009-0083526) through KNRC at Seoul National University. S.J. is supported in part by the NRF grant (2013R1A1A2058449). H.M.L is supported in part by Basic Science Research Program through the NRF grant (2013R1A1A2007919) and by the Chung-Ang University Research Grants in 2014. S.C.P is supported by Basic Science Research Program through the NRF grants (NRF-2011-0029758 and NRF-2013R1A1A2064120).

Appendix A: Approximate Diagonalizations of RPV Masses

Bilinear RPV in superpotential and soft SUSY breaking scalar potential leads to the mixing between neutrinos (charged leptons) and neutralinos (charginos). As such bilinear couplings are required to be small to produce tiny neutrino masses, it is convenient to rotate away first these mixing masses by the following approximate diagonalizations collected from Ref. [14].

(i) Neutrino–neutralino diagonalization:

$$\begin{pmatrix} \nu_i \\ \chi_j^0 \end{pmatrix} \longrightarrow \begin{pmatrix} \nu_i - \theta_{ik}^N \chi_k^0 \\ \chi_j^0 + \theta_{lj}^N \nu_l \end{pmatrix}, \tag{A1}$$

where (ν_i) and (χ_j^0) represent three neutrinos $(\nu_e, \nu_\mu, \nu_\tau)$ and four neutralinos $(\tilde{B}, \tilde{W}_3, \tilde{H}_d^0, \tilde{H}_u^0)$ in the flavor basis, respectively. The rotation elements θ_{ij}^N are given by

$$\begin{aligned} \theta_{ij}^N &= \xi_i c_j^N c_\beta - \epsilon_i \delta_{j3} \quad \text{and} \\ (c_j^N) &= \frac{M_Z}{F_N}\left(\frac{s_W M_2}{c_W^2 M_1 + s_W^2 M_2}, -\frac{c_W M_1}{c_W^2 M_1 + s_W^2 M_2}, -s_\beta \frac{M_Z}{\mu}, c_\beta \frac{M_Z}{\mu}\right), \end{aligned} \tag{A2}$$

where $\xi_i \equiv a_i - \epsilon_i$ and $F_N = M_1 M_2/(c_W^2 M_1 + s_W^2 M_2) + M_Z^2 s_{2\beta}/\mu$. Here $s_W = \sin\theta_W$ and $c_W = \cos\theta_W$ with the weak mixing angle θ_W.

(ii) Charged-lepton–chargino diagonalization:

$$\begin{pmatrix} e_i \\ \chi_j^- \end{pmatrix} \to \begin{pmatrix} e_i - \theta_{ik}^L \chi_k^- \\ \chi_j^- + \theta_{lj}^L e_l \end{pmatrix} \quad ; \quad \begin{pmatrix} e_i^c \\ \chi_j^+ \end{pmatrix} \to \begin{pmatrix} e_i^c - \theta_{ik}^R \chi_k^+ \\ \chi_j^+ + \theta_{lj}^R e_l^c \end{pmatrix}, \tag{A3}$$

where e_i and e_i^c denote the left-handed charged leptons and anti-leptons, $(\chi_j^-) = (\tilde{W}^-, \tilde{H}^-)$ and $(\chi_j^+) = (\tilde{W}^+, \tilde{H}^+)$. The rotation elements $\theta_{ij}^{L,R}$ are given by

$$\begin{aligned} &\theta_{ij}^L = \xi_i c_j^L c_\beta - \epsilon_i \delta_{j2}\ , \quad \theta_{ij}^R = \frac{m_i^e}{F_C} \xi_i c_j^R c_\beta \quad \text{and} \\ &(c_j^L) = -\frac{M_W}{F_C}\left(\sqrt{2}, 2 s_\beta \frac{M_W}{\mu}\right)\ , \\ &(c_j^R) = -\frac{M_W}{F_C}\left(\sqrt{2}(1 - \frac{M_2}{\mu} t_\beta), \frac{M_2^2 c_\beta^{-1}}{\mu M_W} + 2\frac{M_W}{\mu} c_\beta\right), \end{aligned} \tag{A4}$$

and $F_C = M_2 + M_W^2 s_{2\beta}/\mu$.

Appendix B: Bound Estimation

Here we summarize how we reinterpret LHC results to obtain exclusion bounds on our models. We use the next-to-leading order sbottom production cross sections in Refs. [27, 28].

The $bb\nu\nu$ final states are constrained from RPC sbottom pair searches. Sbottoms decaying to $b\chi_1^0$ 100% is currently limited to be above 720GeV [20]. For our given sbottom mass, ignoring differences in cut efficiencies and kinematics, we find the branching ratio suppression needed to make the production rate of the given $\widetilde{b}_1 \widetilde{b}_1^* \to bb\nu\nu$ equal to that of 720GeV sbottom pairs. We reinterpret the stop RPC searches in the $t\bar{t}$+MET channel [22] in the same way to constrain $tt\nu\nu$ final states. For the $\mathrm{LQD}_{113+131}$, the RPC searches of squark pairs can be similarly relevant. Interestingly, a *single* squark pair is weakly constrained from the $q\bar{q}$+MET search [29] to be above only 570 GeV – but they can still exclude small part

of surviving parameter space.

Various $\ell\nu jj$ final states are constrained from leptoquark searches. Leptoquark searches [7, 8] display several set of cuts(signal regions) optimized for different leptoquark masses. For the $\mathrm{LQD}_{113+131}$ which have exactly the same kind of decay modes as leptoquarks, the official CMS exclusion bounds on leptoquarks apply equally well. For the LQD_{i33} and LH_i models which involve heavy quarks in the final states, we carry out Monte-Carlo simulations (based on `MadGraph` [30], `Pythia` [31] and `FastJet` [32]), estimate efficiencies under all displayed cuts and use the most constraining result. To quantify the deviation, we add statistical error, $\sqrt{S+B}$, and the reported systematic errors in quadrature – our own 95%C.L.$\simeq 1.96\sigma$ exclusion bounds on leptoquarks based on this method agree well with the official results. As different signal regions are not mutually exclusive, we do not χ^2 them.

The $ttee$ final states can involve more than three leptons or same-sign dileptons and b-jets which are often clean. We find that multilepton($N_\ell \geq 3$) RPV LLE search [21] with various binned discovery cuts is most relevant to us. We simulate all the discovery cuts with $300 < S_T < 1500$ GeV and use the most stringent result to obtain bounds. The strongest bound is usually from discovery cuts with $\geq 1b$ and $S_T \gtrsim 1000$ GeV requirements. Similar searches of same-sign dileptons plus b-jets plus multijets [33], four-lepton [34] and other $\geq 3\ell$ + b-jet searches in, e.g., Refs. [35] are less optimized for our benchmark models of about 700GeV squarks.

---

[1] https://twiki.cern.ch/twiki/bin/view/AtlasPublic/SupersymmetryPublicResults; https://twiki.cern.ch/twiki/bin/view/CMSPublic/PhysicsResultsSUS.

[2] L. E. Ibanez and G. G. Ross, Nucl. Phys. B **368** (1992) 3.

[3] L. J. Hall and M. Suzuki, Nucl. Phys. B **231** (1984) 419.

[4] W. Buchmuller, R. Ruckl and D. Wyler, Phys. Lett. B **191** (1987) 442 [Erratum-ibid. B **448** (1999) 320].

[5] M. Kuze and Y. Sirois, Prog. Part. Nucl. Phys. **50** (2003) 1 [Erratum-ibid. **53** (2004) 583] [hep-ex/0211048].

[6] G. Aad *et al.* [ATLAS Collaboration], Phys. Lett. B **709** (2012) 158 [Erratum-ibid. **711** (2012) 442] [arXiv:1112.4828 [hep-ex]]; Eur. Phys. J. C **72** (2012) 2151 [arXiv:1203.3172 [hep-ex]]; G. Aad *et al.* [ATLAS Collaboration], JHEP **1306** (2013) 033 [arXiv:1303.0526 [hep-ex]].

[7] CMS Collaboration, CMS-PAS-EXO-12-041.

[8] CMS Collaboration, CMS-PAS-EXO-12-042.

[9] V. Khachatryan *et al.* [CMS Collaboration], arXiv:1408.0806 [hep-ex].

[10] A. Bartl, W. Porod, M. A. Garcia-Jareno, M. B. Magro, J. W. F. Valle and W. Majerotto, Phys. Lett. B **384** (1996) 151 [hep-ph/9606256]. M. A. Diaz, D. A. Restrepo and J. W. F. Valle, Nucl. Phys. B **583** (2000) 182 [hep-ph/9908286]. H. K. Dreiner and S. Grab, Phys. Lett. B **679** (2009) 45 [arXiv:0811.0200 [hep-ph]].

[11] J. A. Evans and Y. Kats, JHEP **1304** (2013) 028 [arXiv:1209.0764 [hep-ph]]. S. Biswas,

D. Ghosh and S. Niyogi, JHEP **1406** (2014) 012 [arXiv:1312.0549 [hep-ph]].

[12] Z. Marshall, B. A. Ovrut, A. Purves and S. Spinner, Phys. Lett. B **732** (2014) 325 [arXiv:1401.7989 [hep-ph]]. Z. Marshall, B. A. Ovrut, A. Purves and S. Spinner, Phys. Rev. D **90** (2014) 015034 [arXiv:1402.5434 [hep-ph]].

[13] Y. Bai and J. Berger, arXiv:1407.4466 [hep-ph]. M. Heikinheimo, M. Raidal and C. Spethmann, arXiv:1407.6908 [hep-ph]. B. A. Dobrescu and A. Martin, arXiv:1408.1082 [hep-ph]. B. Allanach, S. Biswas, S. Mondal and M. Mitra, arXiv:1408.5439 [hep-ph].

[14] E. J. Chun, D. W. Jung, S. K. Kang and J. D. Park, Phys. Rev. D **66** (2002) 073003 [hep-ph/0206030]. D. W. Jung, S. K. Kang, J. D. Park and E. J. Chun, JHEP **0408** (2004) 017 [hep-ph/0407106].

[15] E. J. Chun and S. K. Kang, Phys. Rev. D **61** (2000) 075012 [hep-ph/9909429].

[16] B. Mukhopadhyaya, S. Roy and F. Vissani, Phys. Lett. B **443**, 191 (1998) [hep-ph/9808265]

[17] E. J. Chun and J. S. Lee, Phys. Rev. D **60** (1999) 075006 [hep-ph/9811201]. S. Y. Choi, E. J. Chun, S. K. Kang and J. S. Lee, Phys. Rev. D **60**, 075002 (1999) [hep-ph/9903465].

[18] M. Hirsch, M. A. Diaz, W. Porod, J. C. Romao and J. W. F. Valle, Phys. Rev. D **62**, 113008 (2000) [Erratum-ibid. D **65**, 119901 (2002)] [hep-ph/0004115].

[19] E. J. Chun and S. C. Park, JHEP **0501**, 009 (2005) [hep-ph/0410242].

[20] CMS Collaboration, CMS-PAS-SUS-13-018.

[21] S. Chatrchyan *et al.* [CMS Collaboration], Phys. Rev. Lett. **111**, no. 22, 221801 (2013) [arXiv:1306.6643 [hep-ex]].

[22] CMS Collaboration, CMS-PAS-SUS-14-011.

[23] H. M. Lee, V. Sanz and M. Trott, JHEP **1205** (2012) 139 [arXiv:1204.0802 [hep-ph]].

[24] V. Barger, P. Huang, M. Ishida and W. -Y. Keung, Phys. Lett. B **718** (2013) 1024 [arXiv:1206.1777 [hep-ph]].

[25] S. Heinemeyer, W. Hollik and G. Weiglein, Phys. Rept. **425** (2006) 265 [hep-ph/0412214].

[26] L. J. Hall, D. Pinner and J. T. Ruderman, JHEP **1204** (2012) 131 [arXiv:1112.2703 [hep-ph]].

[27] W. Beenakker, S. Brensing, M. Kramer, A. Kulesza, E. Laenen and I. Niessen, JHEP **1008** (2010) 098 [arXiv:1006.4771 [hep-ph]].

[28] LHC SUSY Cross Section Working Group, https://twiki.cern.ch/twiki/bin/view/LHCPhysics/SUSYCrossSections

[29] CMS Collaboration [CMS Collaboration], CMS-PAS-SUS-13-019.

[30] J. Alwall, M. Herquet, F. Maltoni, O. Mattelaer and T. Stelzer, JHEP **1106**, 128 (2011) [arXiv:1106.0522 [hep-ph]].

[31] T. Sjostrand, S. Mrenna and P. Z. Skands, JHEP **0605**, 026 (2006) [hep-ph/0603175].

[32] M. Cacciari, G. P. Salam and G. Soyez, Eur. Phys. J. C **72**, 1896 (2012) [arXiv:1111.6097 [hep-ph]].

[33] G. Aad *et al.* [ATLAS Collaboration], JHEP **1406**, 035 (2014) [arXiv:1404.2500 [hep-ex]].

[34] G. Aad *et al.* [ATLAS Collaboration], arXiv:1405.5086 [hep-ex].

[35] The ATLAS collaboration, ATLAS-CONF-2013-051.